Volume 12 | Number 22 | 21 November 2025

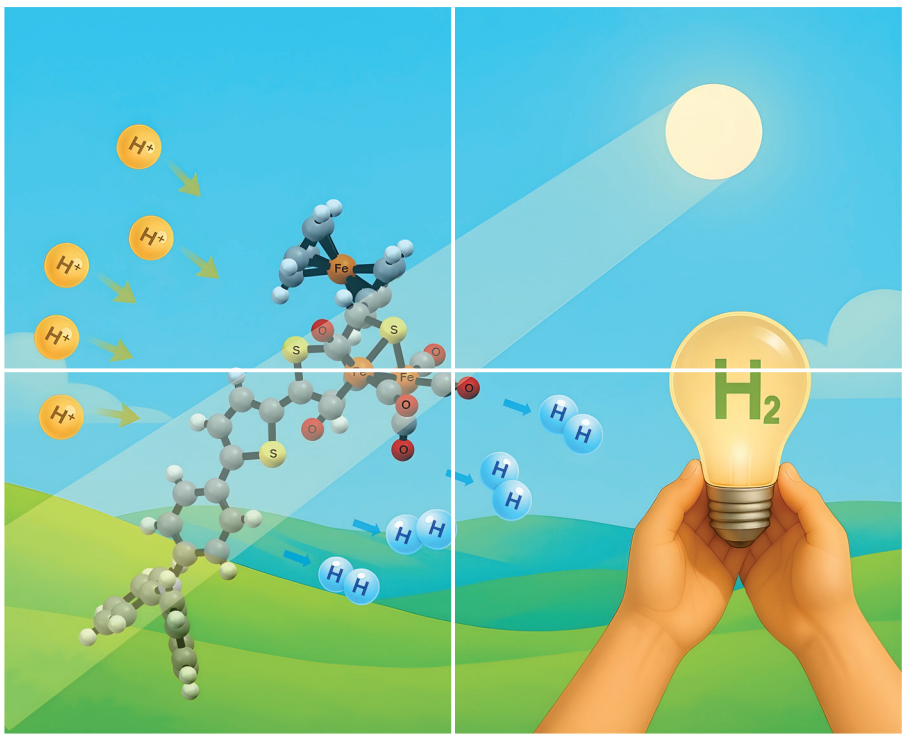

INORGANIC CHEMISTRY

FRONTIERS

CCS 中国化学会 CHINESE CHEMICAL SOCIETY
PEKING UNIVERSITY 1898
ROYAL SOCIETY OF CHEMISTRY
rsc.li/frontiers-inorganic

INORGANIC CHEMISTRY FRONTIERS

RESEARCH ARTICLE

View Article Online
View Journal | View Issue

Cite this: *Inorg. Chem. Front.*, 2025, **12**, 6958

Engineered [FeFe]-hydrogenase mimics featuring heteroaryl linkers: molecular design and photocatalytic hydrogen evolution under visible light

Ibrahim Basma,†[a] Katharina Rediger,†[b] Chizuru Kasahara,[a] Hassan Abul-Futouh, *[c] Mathias Micheel, ‡[b] Micheal K. Farh,§[d] Phil Köhler, [a] Grzegorz Mlostoń, [e] Maria Wächtler *¶[b] and Wolfgang Weigand *[a]

Inspired by the active site of [FeFe]-hydrogenase, we have developed synthetic mimics engineered from the reaction of heteroaryl thioketone derivatives ferrocenyl(5-(4-(diphenylamino)phenyl)thiophen-2-yl) methanethione (**PS-Fc-1**), ferrocenyl(5′-(4-(diphenylamino)phenyl)-[2,2′-bithiophen]-5-yl)methanethione (**PS-Fc-2**) and phenyl(5′-(4-(diphenylamino)phenyl)-[2,2′-bithiophen]-5-yl)methanethione (**PS-Ph**) as pro-ligands with $Fe_3(CO)_{12}$. The resulting complexes contain thiolato ligands, which enable a close linkage between heteroaryl chromophores and the catalytic center, thereby promoting efficient photocatalytic hydrogen evolution under visible light irradiation. These mimics incorporate a push–pull organic chromophore, consisting of triphenylamine and (bi)thiophene groups, designed to facilitate direct photoexcitation into a charge-separated state. Electrochemical properties were examined using cyclic voltammetry, and photophysical characteristics were determined by steady-state spectroscopy and nanosecond transient absorption supported by (TD-)DFT simulations. Whilst both catalytically active species revealed the formation of charge-separated states directly upon excitation, fast deactivation due to relaxation into low-lying ferrocene-located states prevents the formation of long-lived excited states in the ferrocene-linked dyad. This explains the reduced activity for hydrogen generation of the dyad containing the ferrocene moiety compared to the phenyl one.

Received 22nd May 2025,
Accepted 10th September 2025

DOI: 10.1039/d5qi01191d

rsc.li/frontiers-inorganic

Introduction

Energy is considered the keystone for productivity improvement in agriculture and industrial sectors. However, the main energy source for most of the world's energy requirements is governed by fossil fuels, which are the primary drivers of greenhouse gas emissions. Therefore, the search for eco-friendly alternatives to reduce these emissions is progressively becoming a major concern for industrial developers and world governments.[1–3] It is important to consider that any alternative selected should be abundant, affordable, environmentally sustainable, and widely available across regions to effectively compete with traditional fuels. Among the sustainable energy sources, green hydrogen is considered the most viable long-term solution that meets these criteria. Green hydrogen can be produced *via* photocatalysis using visible sunlight as the sole energy source.[4,5] A photocatalytic system is typically achieved through the combination of a catalyst (CAT) and a photosensitizer (PS), with the support of a sacrificial electron donor (SED), to ensure the thermodynamic feasibility of catalytic

[a]*Institute for Inorganic and Analytical Chemistry, Friedrich Schiller University Jena, Humboldtstr. 8, 07743 Jena, Germany. E-mail: wolfgang.weigand@uni-jena.de*
[b]*Department of Chemistry and State Research Center OPTIMAS, RPTU Kaiserslautern-Landau, Erwin-Schrödinger-Str. 52, 67663 Kaiserslautern, Germany*
[c]*Department of Chemistry, Faculty of Science, The Hashemite University, P.O. Box 330127, Zarqa 13133, Jordan. E-mail: h.abulfutouh@hu.edu.jo*
[d]*Department of Chemistry, Faculty of Science, Assiut University, 71515 Assiut, Egypt*
[e]*Department of Organic & Applied Chemistry, University of Łódź, Tamka 12, 91-403 Łódź, Poland*
†These authors contributed equally to this work.
‡Current address: Institute for Technical Chemistry and Environmental Chemistry, Friedrich-Schiller University Jena, Philosophenweg 7a, 07743 Jena, Germany.
§Current address: Center for Energy and Environmental Chemistry Jena (CEEC Jena), Friedrich Schiller University Jena, Philosophenweg 7a, 07743 Jena, Germany.
¶Current address: Institute of Physical Chemistry and Kiel Nano, Surface and Interface Science (KiNSIS), Kiel University, Max-Eyth-Str. 1, 24118 Kiel, Germany. Email: waechtler@phc.uni-kiel.de

reactions while inhibiting unproductive back-electron transfer. In the interest of economic and environmental impact, the most efficient photocatalytic system should be one in which both the CAT and the PS are designed entirely from earth-abundant elements and provide long-term stability and high capacity for hydrogen formation.[6,7] Such photocatalytic systems can be either intermolecular, in which the photoactive unit is separated from the catalyst, or intramolecular, where the photoactive unit is combined with the catalytic center as a single entity.[8] The former is considered less efficient as it is limited by diffusion processes bringing the PS and the CAT close enough to facilitate the transfer of electrons from the excited PS to the CAT center.[8,9–11] A paradigm for a catalyst based on earth-abundant elements is provided by nature. The protein [FeFe]-hydrogenase is recognized as a highly efficient catalyst for hydrogen formation, with a reported turnover frequency (TOF) greater than 10^4 s^{-1} under optimal conditions.[12,13] The structure of the active site (the so-called H-cluster) of [FeFe]-hydrogenase revealed by X-ray crystallographic analysis is presented in Fig. 1.[14–17] As shown in Fig. 1, the topology of the H-cluster contains a butterfly [2Fe2S] subunit acting as the catalytic center for proton reduction and an [4Fe4S] ferredoxin cluster that is responsible for electron transfer to the H-cluster.[14] Inspired by the natural archetype of [FeFe]-hydrogenase, a variety of its mimics have been developed to function as catalysts for the electrochemical reduction of protons.[18–25] Building on this existing knowledge, it is intuitive to explore the potential applications of these mimics as catalysts in photochemical hydrogen production processes. In this context, photochemically driven proton reduction systems have been achieved through the combination of a PS and an [FeFe]-hydrogenase mimic as a CAT.[26–31]

Reviewing the literature on these photochemically driven proton reduction systems, one can find that the PS can be bonded to the CAT using two different strategies, both with concomitant advantages and disadvantages.[31] In the first strategy, the PS is attached to the CAT *via* an organic dithiolato linker, while the second approach relies on introducing the PS directly to one of the iron centers through a ligand as an alternative to one of the terminal CO groups.[28,32–41] Following the first scenario, the group of Sun reported the first example of this strategy in which an acetylene-functionalized ruthenium bis(terpyridine) complex was selected as the PS, and the synthetic model of [FeFe]-hydrogenase, $[Fe_2(CO)_6\{\mu\text{-}(SCH_2)_2NR\}]$ (R = C_6H_5I), was used as the CAT.[32] As a result, the spectroscopic and electrochemical data of their dyad system indicated that oxidative quenching of the photoexcited $*[Ru(terpy)_2]^{2+}$ by the CAT was uphill by 0.59 eV.[42] In subsequent years, further studies on such systems using dyads containing Ru- or Re-based photosensitizers or organic chromophores have been reported and they showed diversity in their turnover number (TON) for light-driven hydrogen evolution.[31] However, the highest TON of 31.8 was observed in a study by Hou and co-workers, in which they synthesized a dyad system by covalently connecting two metal-free PSs and one $[Fe_2S_2]$ cluster.[43] The ongoing development of these scenarios has led our group to design a new class of dyads that absorb light in the UV region. This includes a small, compact, heavy-metal-free photosensitizer–catalyst dyad by utilizing a silicon-containing heteroaromatic system.[44,45] In this study, a TON of 539 was reached after 7 hours of irradiation under optimal conditions, and hence it was considered the highest reported value at that time for such small, compact systems. More recently, we have designed another prototype dyad comprising π-conjugated oligothiophenes as light absorbers, which shows a remarkable long-term photocatalytic activity among the reported analogous complexes in the visible spectral range.[46] Considering these remarkable findings and our ongoing interest in the reaction of heteroaryl thioketones with $Fe_3(CO)_{12}$, we aimed to design photoactive thioketone derivatives that are good at absorbing visible light.[24,47,48] These derivatives can react with $Fe_3(CO)_{12}$ to form [FeFe]-hydrogenase-mimicking complexes that can be activated by visible light. The thioketones developed in this study are composed of three essential components: (i) the thiocarbonyl group, (ii) a ferrocenyl moiety, and (iii) a push–pull organic chromophore based on triphenylamine and (bi)thiophene aimed at direct photoexcitation into a charge-separated state. The thiocarbonyl group is regarded as the reactive site for coordination with the metal center and the good donor ability of the ferrocenyl group is expected to enhance the electron density in such a system, supporting the reactivity for coupling and increasing stability. Furthermore, the ferrocenyl moiety could act as an intrinsic electron donor, thereby supporting the formation of a charge-separated state and charge carrier accumulation at the [FeFe] center.[49–53] The resulting [FeFe]-hydrogenase-mimicking complexes are investigated for their photocatalytic hydrogen generation ability under visible light. Additionally, to evaluate the impact of the ferrocenyl moiety, which can act as an electron donor but also as an energy acceptor, a structural analogue featuring a phenyl ring in place of the ferrocenyl group was synthesized.[54] Moreover, the known compound 4-([2,2′-bithiophen]-5-yl)-*N*,*N*-diphenylaniline (**PS**) was synthesized for comparison, following the method previously reported in the literature.[55]

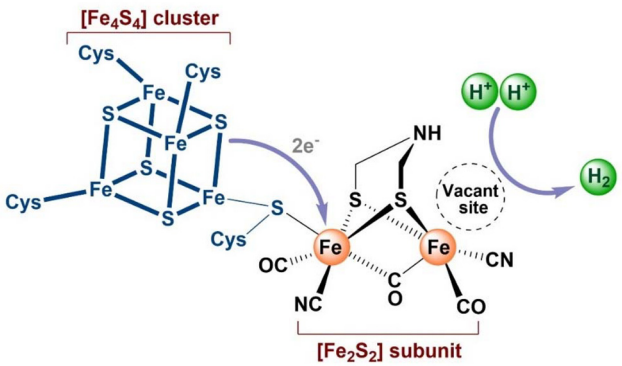

Fig. 1 The active site of natural [FeFe]-hydrogenase.

Results and discussion

Synthesis and characterization

The synthetic routes for obtaining the target systems are outlined in Scheme 1. Initially, the reaction of ferrocenecarboxylic acid with 2-bromothiophene or 5-bromo-2,2′-bithiophene in CH_2Cl_2 solution produced compounds **1** and **2**, respectively, as shown in Scheme 1 (first step).

In parallel, the reaction of benzoic acid with 5-bromo-2,2′-bithiophene under the same conditions afforded compound **3** (Scheme 1, first step). In the subsequent step, compounds **1–3** were reacted with *N*,*N*-diphenyl-4-(tributylstannyl)aniline, respectively, in the presence of $Pd(PPh_3)_4$ as a catalyst, resulting in the formation of the desired compounds **4–6**, respectively, as depicted in Scheme 1 (second step). Compounds **1–6** were characterized by means of ^1H and $^{13}C\{^1H\}$ NMR spectroscopic techniques as well as elemental analysis, mass spectrometry and single-crystal X-ray structure determination of compound **4** (Fig. S1, SI), which are described in detail in the SI. The next step involved thionating the carbonyl groups in compounds **4–6** using Lawesson's reagent in THF at 65 °C for 4 hours, resulting in compounds **PS-Fc-1**, **PS-Fc-2**, and **PS-Ph**

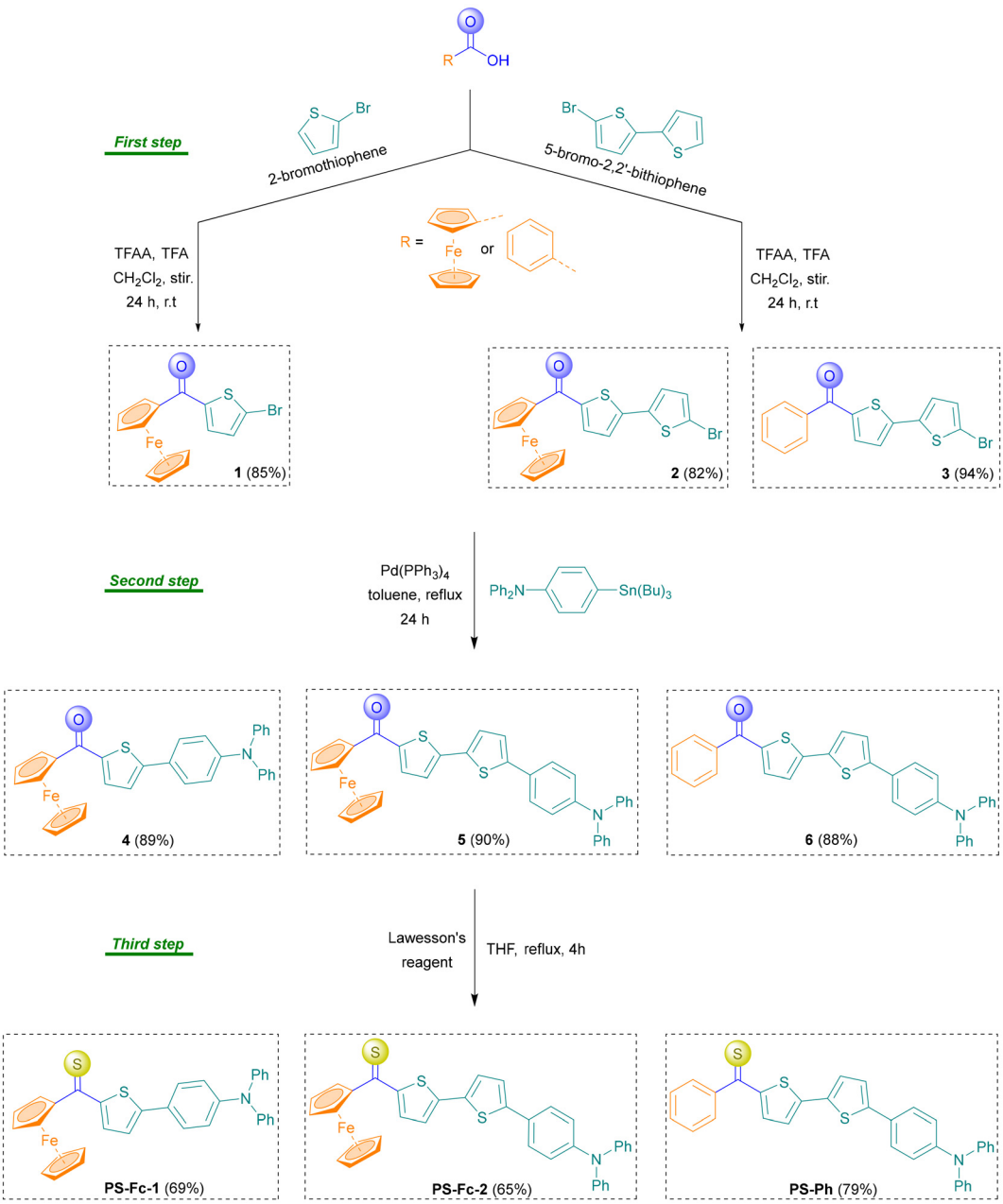

Scheme 1 Preparation of compounds **1–6** and **PS-Fc-1**, **PS-Fc-2**, and **PS-Ph**. First step: Friedel–Crafts acylation. Second step: Stille coupling. Third step: thionation using Lawesson's reagent.

with moderate yields, as shown in Scheme 1 (third step). The obtained compounds were characterized by spectroscopic techniques (^{1}H and ^{13}C{^{1}H} NMR, Fig. S14–S19, SI), IR (Fig. S41–43, SI), mass spectrometry (Fig. S31–33, SI), and elemental analysis. The absence of signals corresponding to the ketone group in the ^{13}C{^{1}H} NMR spectra of compounds **PS-Fc-1**, **PS-Fc-2**, and **PS-Ph** along with the appearance of a signal around 220 ppm for the carbon atoms of the thioketone group confirmed the postulated structures of these compounds.

Synthesis and characterization of diiron complexes

Treatment of equimolar amounts of $Fe_3(CO)_{12}$ and compounds **PS-Fc-1**, **PS-Fc-2**, and **PS-Ph** in boiling THF for 2 hours, followed by column chromatography, afforded complexes **PS-Fc-CAT-1**, **PS-Fc-CAT-2**, **PS-Fc-CAT-3**, and **PS-Ph-CAT** with isolated yields ranging from 27% to 46%, as depicted in Scheme 2. Notably, only compound **PS-Fc-2** produced a mixture of *ortho*-metalated complexes **PS-Fc-CAT-2** and **PS-Fc-CAT-3** under similar conditions (Scheme 2). This behavior has been previously observed in similar reactions of thioketone derivatives with $Fe_3(CO)_{12}$, as reported by our group.[30,47] The new complexes were characterized by ^{1}H and ^{13}C{^{1}H} NMR, IR, UV-Vis spectroscopy, mass spectrometry, elemental analysis, cyclic voltammetry, and X-ray crystallography for complex **PS-Fc-CAT-2.**

The IR spectra of complexes **PS-Fc-CAT-1**, **PS-Fc-CAT-2**, and **PS-Ph-CAT** (Fig. S44, 45 and 47, SI) reveal three absorption bands located at 2068, 2027, and 1987 cm^{-1} (for **PS-Fc-CAT-1**); 2068, 2029, and 1990 cm^{-1} (for **PS-Fc-CAT-2**); and 2070, 2031, and 1994 cm^{-1} (for **PS-Ph-CAT**), corresponding to the terminal CO ligands. In contrast, the IR spectrum of complex **PS-Fc-CAT-3** (Fig. S46, SI) shows four characteristic metal/carbonyl stretching bands located at 2043, 2035, 2000, and 1946 cm^{-1}. The obtained results are consistent with those of the corresponding iron complexes reported in the literature.[30,47] It is noteworthy that the frequencies of complex **PS-Ph-CAT** are slightly shifted to higher values compared to those of complexes **PS-Fc-CAT-1** and **PS-Fc-CAT-2**, indicating a weaker electron-donating character of the phenyl ring to the FeFe center compared to the ferrocene one.

The ^{1}H NMR spectra of complexes **PS-Fc-CAT-1**, **PS-Fc-CAT-2**, and **PS-Ph-CAT** (Fig. S20, 22 and 26, SI) display a singlet resonance that is related to the methine moieties in the region of 5.40–5.57 ppm. However, this resonance is completely absent in the spectrum of **PS-Fc-CAT-3** (Fig. S24, SI), indicative

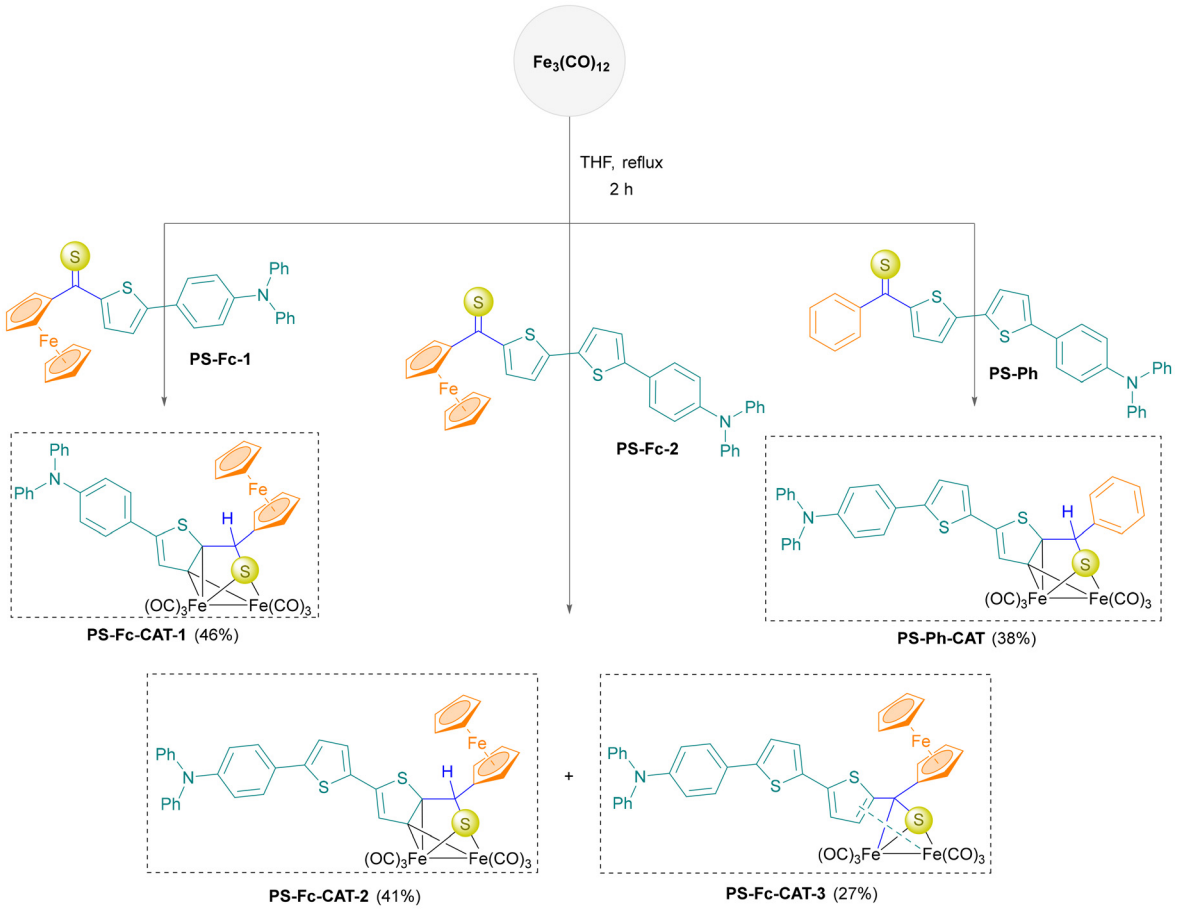

Scheme 2 Synthetic routes of complexes **PS-Fc-CAT-1–3** and **PS-Ph-CAT**.

of a distinct alteration in its structure. Moreover, nine protons of the ferrocene moiety in complexes **PS-Fc-CAT-1–3** were also detected in the area between 3.21 and 4.74 ppm. The signals of the other protons, which confirmed the proposed structures of the obtained complexes, were also detected within the expected range. The $^{13}C\{^1H\}$ NMR spectrum of **PS-Fc-CAT-3** (Fig. S25, SI) displays a distinct singlet resonance at approximately 179.0 ppm, which is absent in the spectra of **PS-Fc-CAT-1**, **PS-Fc-CAT-2**, and **PS-Ph-CAT** (Fig. S21, 23 and 27, SI). This resonance is attributed to the carbon atom adjacent to the ferrocene moiety and hence provides strong support for the proposed structure of **PS-Fc-CAT-3**. Additionally, all complexes show signals of the terminal carbonyl carbon atoms of the iron cores in the range of 209.0–213.0 ppm (Fig. S21, 23, 25 and 27, SI).

The molecular structure of complex **PS-Fc-CAT-2** was unambiguously determined through single-crystal X-ray diffraction, and its molecular geometry is depicted in Fig. 2. A suitable single crystal of complex **PS-Fc-CAT-2** was successfully obtained through the diffusion of pentane into a CH_2Cl_2 solution of complex **PS-Fc-CAT-2** at a low temperature (−20 °C). It is evident from Fig. 2 that the thiolato ligand in complex **PS-Fc-CAT-2** is bound to the two iron centers *via* the sulfur atom, with an average Fe–S bond length of 2.2552(7) Å, which is consistent with those of analogous complexes reported in the literature.[30,47]

Moreover, complex **PS-Fc-CAT-2** features a σ-bond to one iron atom (Fe1) through the β-carbon of the thiophene ring, directly bonded to the thiolato moiety, while the other iron atom (Fe2) is π-coordinated to the α- and β-C atoms of the same thiophene ring in an η^2-mode. The Fe–Fe bond length in complex **PS-Fc-CAT-2** (2.5311(6) Å) is comparable to those of similar complexes described in the literature.[30,47] The average Fe–CO bond length in complex **PS-Fc-CAT-2** (1.7937(3) Å) aligns with those observed for analogous complexes reported in the literature.[30,47] The ferrocene moiety in complex **PS-Fc-CAT-2** adopts an eclipsed conformation.

The electrochemical behavior of the resulting complexes was investigated by applying cyclic voltammetry in CH_2Cl_2-$[n\mathrm{Bu}_4\mathrm{N}][\mathrm{BF}_4]$ solution at a scan rate of 0.2 V s^{-1} (V referenced to the Fc^+/Fc couple).

As indicated in Fig. 3, the cyclic voltammogram of each complex exhibited two reversible couples in the reduction region at $E_{1/2}$ = −1.49 and −1.78 V (for **PS-Fc-CAT-1**), $E_{1/2}$ = −1.48 and −1.77 V (for **PS-Fc-CAT-2**), $E_{1/2}$ = −1.28 and −1.79 V (for **PS-Fc-CAT-3**), and $E_{1/2}$ = −1.45 and −1.71 V (for **PS-Ph-CAT**). These two reversible couples can be assigned to the Fe^I–$Fe^I \rightarrow Fe^I$–Fe^0 couple and Fe^I–$Fe^0 \rightarrow Fe^0$–Fe^0 couple, respectively. This behavior is similar to that of its analog reported in the literature, and the reduction values of these complexes are shifted to lower values compared to those of the analog.[30]

Photocatalytic activities

The photocatalytic H_2 production activities of the molecular dyad (**PS-CAT** without Fc) as well as the molecular triad (**PS-CAT** with Fc) were investigated under visible light irradiation. Initially, in order to determine the excitation wavelength of **PS-CAT**s, the UV-vis absorption of the complexes was recorded in CH_2Cl_2. **PS-Fc-CAT-2**, **PS-Fc-CAT-3**, and **PS-Ph-CAT** (Fig. S48, SI) showed strong absorption bands around 393, 651, and 390 nm, respectively. Contrarily, complex **PS-Fc-CAT-1** absorbs radiation only in the UV region (Fig. S48, SI) in accordance with the size of the conjugated system of the chromophoric oligothiophene unit. Accordingly, **PS-Fc-CAT-2**, **PS-Fc-CAT-3**, and **PS-Ph-CAT** were tested for their hydrogen evolution activity. For this purpose, photocatalysis under visible light irradiation in the presence of BIH (1,3-dimethyl-2-phenylbenzimidazoline) as both the electron and proton source was performed. **PS-Fc-CAT-2** and **PS-Ph-CAT** showed catalytic activity under 405 nm irradiation. In contrast, **PS-Fc-CAT-3** was inactive for hydrogen evolution under 625 nm irradiation, which agrees with observations recently reported for a related system with a diene linker between the sensitizer and the catalyst

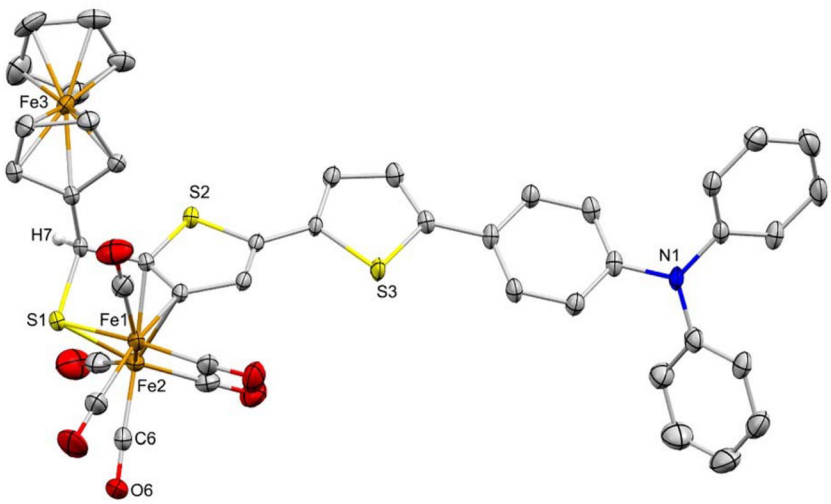

Fig. 2 Molecular structure of compound **PS-Fc-CAT-2** in the crystal. Displacement ellipsoids are drawn at the 50% probability level, and H-atoms are omitted for clarity.

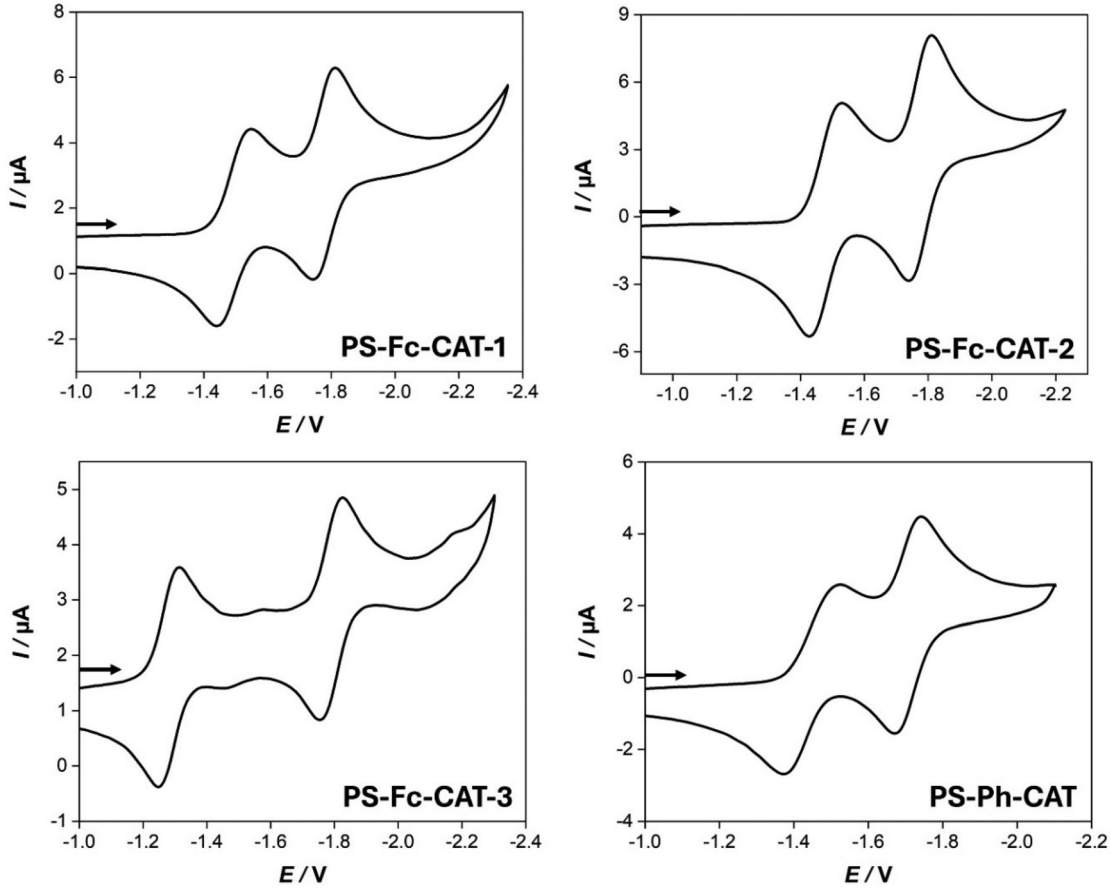

Fig. 3 Cyclic voltammetry of 1.0 mM of complexes **PS-Fc-CAT-1–3** and **PS-Ph-CAT** in CH_2Cl_2-[nBu$_4$N][BF_4] (0.1 M) solutions at a 0.2 V s^{-1} scan rate using a glassy carbon disk (d = 1.6 mm). The arrows indicate the scan direction. The potentials E are given in V and referenced to the Fc^+/Fc couple.

unit.[47] Fig. 4 shows the time profile of H_2 evolution for **PS-Fc-CAT-2** and **PS-Ph-CAT**. The turnover numbers (TONs) after 20 h of irradiation reached ~294 and ~112 for **PS-Ph-CAT** and **PS-Fc-CAT-2**, respectively. It is noteworthy that the turnover frequencies (TOF) for the initial 2 hours of irradiation were ~55.4 h^{-1} for the dyad and ~2.6 h^{-1} for the triad. However, the triad showed superior catalytic stability, *i.e.*, **PS-Ph-CAT** lost its catalytic activity after 12 hours of irradiation, though **PS-Fc-CAT** kept producing H_2 beyond this period. The findings indicated that the Fc moiety provided catalytic stability; however, it exerted a negative influence on the catalytic efficiency of the triad. Nevertheless, compared to our previously reported [FeFe]-hydrogenase mimics with visible activity, the TOF of **PS-Ph-CAT** was significantly higher.[46,47] This phenomenon suggests that the thioketone structure provides **PS-CAT** with unique photoexcited properties. In order to gain insights into the photoexcited states of dyads and triads and the underlying reasons for their efficiency and stability, nanosecond transient absorption (ns-TA) spectroscopy of **PS-Ph-CAT** and **PS-Fc-CAT-2** was performed.

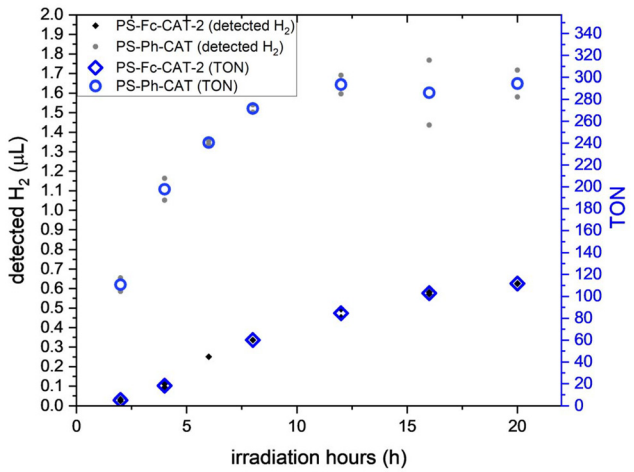

Fig. 4 Time profile of photocatalytic H_2 production and the TONs of **PS-Fc-CAT-2** and **PS-Ph-CAT**. The catalyst concentrations were 100 µM and the BIH concentrations were 10 mM in the acetonitrile/*N*-methyl-2-pyrrolidone = 1/3 mixture under 405 nm irradiation.

Properties of excited states in PS-CAT dyads

To explore the manifold of excited states and analyze the excitation conditions, the absorption spectra of the dyads **PS-Ph-CAT** and **PS-Fc-CAT-2** are compared to a model sensitizer **PS**. Upon linking the catalysts to the sensitizer **PS**, slight character-

istic changes in the absorption and emission properties are observed (Fig. 5). The absorption spectrum of the sensitizer unit **PS** shows two absorption features at 305 nm ($\varepsilon = 4.4 \times 10^4$ L mol^{-1} cm^{-1}) and 379 nm ($\varepsilon = 8.3 \times 10^4$ L mol^{-1} cm^{-1}) and a broad, intense emission band at 459 nm, which is independent of the excitation wavelength (Fig. S51, SI). The absorption spectra and, thus, the electronic structure of the modified sensitizer species **PS-Fc-2** and **PS-Ph** acting as precursors for the dyads were revealed to be heavily influenced by the additionally introduced thioketone functionality. Although changes in the photophysical properties due to the linkage of either the phenyl or ferrocenyl groups are evident in the absorption spectra, the absorption features of the dyads are more comparable to the unsubstituted sensitizer **PS**. Hence, once the reaction center is linked to the sensitizers to form **PS-Fc-CAT-2** and **PS-Ph-CAT**, the absorption spectra more closely resemble **PS** than the thioketone form of the sensitizers. The catalyst **PS-Ph-CAT** reveals a split UV absorption feature with peaks at 283 nm ($\varepsilon = 2.9 \times 10^4$ L mol^{-1} cm^{-1}) and 301 nm ($\varepsilon = 2.8 \times 10^4$ L mol^{-1} cm^{-1}) and a peak at 390 nm ($\varepsilon = 2.8 \times 10^4$ L mol^{-1} cm^{-1}) in the UV region. Additionally, a pronounced shoulder in the visible absorption region develops at 482 nm ($\varepsilon = 1.0 \times 10^4$ L mol^{-1} cm^{-1}). The absorption spectrum of the ferrocene-containing catalyst **PS-Fc-CAT-2** exhibits two strong bands at 303 nm ($\varepsilon = 3.1 \times 10^4$ L mol^{-1} cm^{-1}) and 393 nm ($\varepsilon = 3.8 \times 10^4$ L mol^{-1} cm^{-1}) with the latter one, similar to **PS-Ph-CAT**, extending into a shoulder up to 600 nm. The emission intensity is strongly quenched in both dyads and both systems show only a weak emission band with a peak at around 490 nm and a second strongly red-shifted broad feature (Fig. S51, SI). This indicates that the presence of the catalyst quenches the emitting state and the residual emission in the dyad is further reduced by the presence of the ferrocene unit.

To explore the character of the electronic states responsible for light absorption, TD-DFT calculations (for details on the theoretical methods and calculations, see SI) were performed (Fig. 5). The calculated UV-vis absorption spectrum of **PS** allows the assignment of the strong absorption feature at 379 nm in the experimental spectrum of **PS** to a strongly dipole-allowed transition to the S_1 state ($f = 1.08$), which mainly contains contributions of the HOMO to LUMO transition with $^1\pi\pi^*$ character. Excitation to the S_1 state leads to a decreased electron density at the amine nitrogen atom and a subsequent increase at the thiophene units and thus shows slight push–pull character induced by the electron-rich triphenylamine unit, although **PS** does not contain a strong acceptor group.[56,57] The weaker absorption band at 305 nm is represented by the calculated transitions to the S_3 and S_4 states

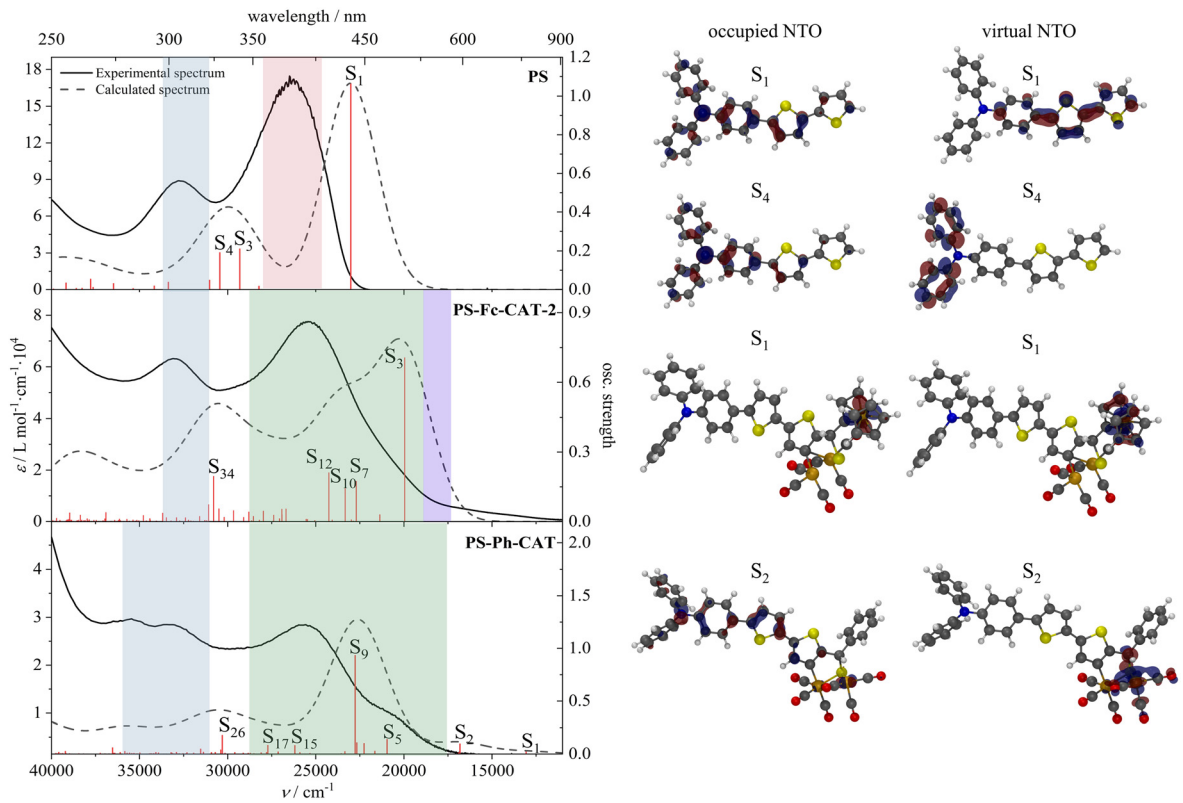

Fig. 5 Experimental (solid line) and calculated (dashed line) UV-vis spectra of **PS** (top), **PS-Fc-CAT-2** (middle), and **PS-Ph-CAT** (bottom) with the calculated vertical transition energies and oscillator strengths indicated as red bars. Regions assigned to transitions isolated at certain functional groups are highlighted in grey, push–pull transitions from the triphenylamine unit to the thiophene unit in red, ferrocenyl-centered transitions in violet, and charge-transfer (CT) transition from the sensitizer to the [FeFe] center in green. The most important transitions of each spectrum are represented as NTOs (natural transition orbitals) on the right.

(f = 0.22 and f = 0.19, respectively) with contributions of both the thiophene and triphenylamine units in the initial as well as the final state with $^1\pi\pi^*$ character. In the dyad and triad, the character of these short wavelength transitions remains basically unchanged, while the push–pull transition appears red-shifted compared to **PS** in accordance with the red shift in the experimental absorption spectra and shows increased push–pull character with the catalyst unit acting as an acceptor. Hence, in the dyad and triad, these transitions possess direct charge-transfer character from the sensitizer unit to the catalyst (Fig. 5). However, the most prominent differences in the **PS-Ph-CAT** and **PS-Fc-CAT-2** electronic transitions can be found in the energetically low-lying shoulders in the visible range of the absorption spectra. In the ferrocenyl-linked triad, **PS-Fc-CAT-2**, the extension of this shoulder can be assigned to the two energetically lowest weak transitions S_1 and S_2 at 550 nm ($f = 1.00 \times 10^{-4}$ and $f = 2.55 \times 10^{-5}$, respectively). Both transitions are exclusively located at the ferrocene moiety, being isolated from the [FeFe]-center and the sensitizing unit. The low oscillator strength of the energetically lower excited states S_1 and S_2 is in line with the observed decreased emission intensity compared to **PS** and is also evident in the emission spectra of ferrocenyl-linked sensitizer species **PS-Fc-2**. Compared to the phenyl-linked dyad **PS-Ph-CAT**, the transitions S_1 and S_2 (f = 0.03 and f = 0.10, respectively) are located at the [FeFe]-center with contributions of the sensitizer unit, indicating some shifting of electron density from the light-harvesting unit to the catalytically active center. Additionally, transition S_5 (f = 0.14) also assigned to the shoulder in the visible range of **PS-Ph-CAT**'s experimental absorption spectrum, is of push–pull character with the [FeFe]-center as the electron density acceptor and the light-harvesting sensitizer unit acting as the donor. Also, the triad **PS-Fc-CAT-2** facilitates these push–pull transitions, as resembled by excitation into the S_3, S_{10} and S_{12} states (f = 0.71, f = 0.14 and f = 0.21, respectively).

As a result, such strong optically allowed transitions with push–pull nature could be a source of efficient charge separation and, thus, high catalytic activity. Besides the presence of transitions with strong direct charge transfer, additional [FeFe]-centered low-lying states are present and could be a possible deactivation pathway. Furthermore, the ferrocenyl-linked triad revealed the lowest states to be ferrocene-centered, which could be a source of additional deactivation of photocatalytically active excited states *via* relaxation of these states by energy transfer to the Fc unit.[58–61] This hypothesis is in line with the observed strong quenching of the singlet excited state in the ferrocene-linked compounds and the slightly quenched emission in the [FeFe]-linked dyads.

Previous studies on thiophene-based hydrogenase mimics indicate that long-lived triplet states of oligothiophenes play a crucial role in the activation mechanism leading to catalytic activity.[46,62] To elucidate whether this is also the case in the newly developed dyads, nanosecond transient absorption spectroscopy was performed to probe the triplet states formed in oligothiophene chromophores *via* intersystem crossing. As expected, the sensitizer **PS** exhibits broad excited state absorption (ESA) with an absorption maximum at 600 nm (Fig. 6). The transient absorption signal decays mono-exponentially with a lifetime of τ = 29.0 ± 0.13 μs. This feature can be assigned to the thiophene-located $^3\pi\pi^*$ state, also in good agreement with TD-DFT calculations (Fig. S53, SI) and with previous results reported in the literature.[46,62] Unfortunately, due to the instability of **PS-Ph-CAT** under the conditions of the ns-TA measurements, the excited state lifetime could only be estimated from a measurement at a single probe wavelength of 600 nm (Fig. 6). At 600 nm, a potentially residual signal from the $^3\pi\pi^*$ sensitizer-centered excited state, as observed for **PS**, can be detected with a lifetime estimated to be 38.3 ± 2.27 μs. Nevertheless, the influence of photoproducts caused by degradation of the dyad cannot be excluded. For the triad **PS-Fc-CAT-2**, which is stable under the measurement conditions, no long-lived sensitizer triplet state can be detected at all (Fig. 6). These findings for **PS-Ph-CAT** and **PS**, together with the strong quenching of the singlet state emission in both species, indi-

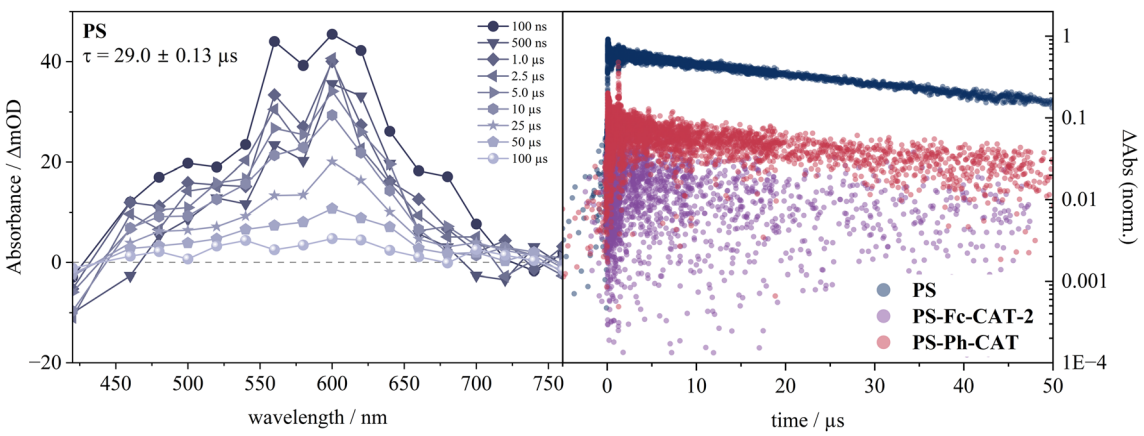

Fig. 6 Nanosecond transient absorption spectra of 21 μM **PS** solution in CH_2Cl_2 at different time delays (left) and kinetic decays at 600 nm of 21 μM **PS**, 27 μM **PS-Fc-CAT-2** and 20 μM **PS-Ph-CAT** normalized by the absorbance of **PS** at λ_{exc} = 440 nm (right).

cate that the formation of a **PS**-localized $^3\pi\pi^*$ triplet state probably does not take place in this case and that a fast alternative channel already occurring from the singlet state is active in these systems. This could be related to the changed character of the excited singlet states, changing the character of the visible absorption from $\pi\pi^*$ to a charge transfer state, directly inducing charge separation between the sensitizer and the catalyst. Furthermore, the presence of [FeFe]-centered low-lying states opens the possibility for the population of these states, providing a general loss channel. In **PS-Fc-CAT-2**, additionally, the population and formal excitation energy transfer to the Fc unit increase this effect.[63] All four processes can be the source of the absence of any long-lived triplet signature, either preventing the formation of the triplet in the first place or quickly quenching this state. The process transferring excitation to the Fc unit, only present in **PS-Fc-CAT-2**, could be responsible for the decreased activity compared to **PS-Ph-CAT**. This interpretation is supported by the location of the spin density of the lowest excited triplet state, being centered at the catalytically active [FeFe]-center in the **PS-Ph-CAT** dyad (Fig. S70, SI), but being located at the inactive ferrocene (Fig. S74, SI) in the **PS-CAT-Fc-2** species. Also, measurements in the presence of the electron donor BIH were conducted and delivered no sign of any long-lived species for the **PS-Fc-CAT-2** species with a reduced $[Fe^0Fe^I]$-center. This indicates that both the charge-separated state and doublet-state ESA of **PS-Fc-CAT-2** occur on time scales below the measurement range, potentially further influenced by the proton-donating ability of BIH forming protonated intermediates.

Activation, reduction and hydrogen evolution pathway of PS-Ph-CAT and PS-Fc-CAT-2

In the light of the data presented, we suggest the following mechanism to explain the activity of the system. The results from the analysis of the singlet excited state manifold indicate a drastic change in the character of the visible absorption features, revealing a unique charge density shifting transition of CT character, with the triphenylamine group acting as an electron-rich donor unit and the [FeFe]-hydrogenase mimic as an acceptor. This results in **PS-Ph-CAT** undergoing direct charge separation already upon excitation, transferring electron density towards the catalyst. This could be the reason for the observed increased catalytic activity compared to previously reported systems, where $\pi\pi^*$ excitation of the sensitizer's thiophene unit is followed by ISC, and charge transfer occurring from the triplet-state manifold is a necessary step. This process is bypassed in the reported systems *via* a direct push–pull transition, which transfers charge carriers from the sensitizer to the catalyst directly. This is in agreement with the observation of a strong quenching of the emission from the singlet sensitizer state. Nevertheless, the singlet excited charge transfer state is not the lowest state in the system, and [FeFe]-centered states are also present and could be a source of radiationless deactivation. If the population of such states could be prevented, a further increase in catalytic activity is expected to occur. The ferrocene unit in **PS-Fc-CAT-2** causes further quenching of emission and additionally reduces the catalytic activity compared to **PS-Ph-CAT**. This indicates a significant interference of the ferrocene unit. There are two known pathways for the quenching mechanism: one including an energy transfer step and a second one with electron transfer from the donor ferrocene to an acceptor.[46,62] Energy transfer to the ferrocene and subsequent thermal relaxation populates a catalytically inactive state, while ferrocene acting as an electron donor would be expected to activate the system either *via* reductive quenching of the **PS** unit in **PS-Fc-CAT-2**, supporting subsequent electron transfer to the catalyst from the reduced sensitizer, or in the case of direct charge transfer as observed in our system, preventing recombination by reduction of the formally oxidized **PS**.[61] The decreased activity for hydrogen evolution of the Fc-containing triad suggests that the energy transfer pathway is active and although the triad **PS-Fc-CAT-2** shows increased stability, the activity for hydrogen evolution is decreased.

Conclusion

In summary, we have developed a series of new photoactive thioketones, **PS-Fc-1**, **PS-Fc-2**, and **PS-Ph**, which react with $Fe_3(CO)_{12}$ to form [FeFe]-hydrogenase mimicking complexes, namely **PS-Fc-CAT-1**, **PS-Fc-CAT-2**, **PS-Fc-CAT-3**, and **PS-Ph-CAT**. These complexes were thoroughly characterized using various analytical techniques, including ^{1}H and $^{13}C\{^1H\}$ NMR, IR spectroscopy, mass spectrometry, and elemental analysis, with X-ray crystallographic analysis performed on **PS-Fc-CAT-2**. By integrating a thiocarbonyl group, a ferrocenyl or phenyl moiety, and a push–pull organic chromophore, these systems were strategically engineered for direct photoexcitation into a charge-separated state. Furthermore, their potential for photocatalytic hydrogen evolution under visible light irradiation was explored. Among the synthesized complexes, only **PS-Fc-CAT-2** and **PS-Ph-CAT** exhibited catalytic activity under 405 nm irradiation. Furthermore, the ferrocenyl-linked dyad revealed decreased activity compared to **PS-Ph-CAT**, indicating a deactivating rather than activating influence of the ferrocene. This is in line with the observed quenched emission and absent ns-TA signal upon linkage of the ferrocene to the dyad, which is due to low-lying Fc-centered excited states causing fast deactivation of the catalyst. However, the incorporation of the ferrocenyl unit can be justified by its ability to enhance the overall stability of the system, thereby contributing to the development of a more durable catalyst for future applications. In contrast, the increased catalytic activity of **PS-Ph-CAT** can be explained by the population of a charge transfer state that transfers electron density from the sensitizer to the catalyst directly upon light excitation.

The present work once again demonstrates the practical usefulness of ferrocenyl thioketones for the synthesis of diverse ferrocenyl-functionalized compounds, which are important for the preparation of medicinally relevant compounds, *e.g.* ferrocifenes, as well as for materials chemistry.[64–68]

Experimental part

Materials and techniques

All manipulations concerning the preparation of all complexes were performed using standard Schlenk and vacuum-line techniques under an inert gas (Ar). The ^{1}H and $^{13}C\{^{1}H\}$ NMR spectra were recorded with a Bruker Avance 400 or 600 MHz spectrometer. Chemical shifts are given in parts per million with references to internal $SiMe_4$ (^{1}H, $^{13}C\{^{1}H\}$). The mass spectrum was recorded with a Finnigan MAT SSQ 710 instrument. Elemental analysis was performed with Leco CHNS-932 apparatus. TLC was performed using Merck TLC aluminum sheets (Silica gel 60 F254). Solvents from Fisher Scientific and other chemicals from Acros and Aldrich were used without further purification. All solvents were dried and distilled prior to use according to standard methods. Compound **PS** was synthesized according to the procedure reported in the literature.[55] The synthetic procedures and characterization of compounds **1–6** are described in detail in the SI.

Electrochemistry

Corrections for the *iR* drop were performed for all experiments. CV measurements were conducted using a three-electrode technique [glassy carbon disk (diameter = 1.6 mm) as the working electrode, Ag/Ag^{+} in MeCN as the reference electrode, and a Pt wire as the counter electrode] using a Reference 600 Potentiostat (Gamry Instruments). All experiments were performed in CH_2Cl_2 solutions (concentration of the complexes: 1.0 mM) containing 0.1 M [nBu$_4$N][BF_4] at room temperature. The solutions were purged with N_2 and a stream of N_2 was maintained over them during the measurements. The vitreous carbon disk was polished on a felt tissue with alumina before each measurement. All potential values reported in this work are referenced to the potential of the ferrocenium/ferrocene (Fc^{+}/Fc) couple.

Crystal structure determination

The single-crystal X-ray intensity data for the reported compounds were collected on a Bruker-Nonius Kappa-CCD diffractometer equipped with a Mo-Kα IμS microfocus source and an Apex2 CCD detector at T = 120(2) K. The crystal structures were solved with SHELXT-2018/3 and refined by full-matrix least-squares methods on F^2 with SHELXL-2018/3 using the Olex2 1.3 environment.[69–71] Multi-scan absorption correction was applied to the intensity data.[72] Restraints on interatomic distances and anisotropic displacement parameters were used for the disordered C_4S ring in compound **4** (SADI and SIMU commands in SHELXL).[70] CCDC 2445996 (for **PS-Fc-CAT-2**) and 2445997 (for **4**) contain the supplementary crystallographic data for this paper (see Table S1).

Steady-state spectroscopy

UV-vis absorption spectroscopy was carried out with a SPECORD S600 (Analytik Jena) and a Lambda 900 double-beam spectrometer (PerkinElmer). Emission spectroscopy was performed with a Fluorolog 3-22τ spectrometer (Horiba Jobin Yvon).

Nanosecond transient absorption spectroscopy

The time-resolved transient absorption spectra on a nanosecond timescale were recorded on a custom-built pump–probe transient absorption setup. A 10 Hz Nd:YAG laser (Continuum Surelite) with a 5 ns pulse width was used to pump the excited state. The fundamental (1064 nm) passes a second-harmonic generation step (532 nm) followed by a third-harmonic generation step to gain the frequency-tripled wavelength (355 nm). This beam is transmitted to an optical parametric oscillator (Continuum Surelite) generating tunable wavelengths from 400 nm to 650 nm with energies ranging from 15 mJ to 80 mJ. If not stated otherwise, an excitation wavelength of 440 nm and a pulse energy of 20 mJ were used. To record the ground state's transmission and probe the excited state, a 75 W xenon arc lamp (pulsed or CW) was used. By focusing the beam path with a concave mirror onto the sample, the transmitted light is spectrally dispersed (Acton Princeton Instrument 2300), detected by a photomultiplier tube (Hamamatsu R928) and processed (Pascher Instruments AB).

Light-driven hydrogen evolution reactions

All photocatalytic reactions were performed with a 3D-printed photoreactor utilizing a 405 nm LED from LEDENGIN (LZ4-00UB0R).[46] The samples were prepared in LABSOLUTE clear glass screw neck vials (ND13) and screw seals (ND13, butyl red/PTFE grey) (total volume: 5 mL) under a nitrogen atmosphere. **PS-CAT** and BIH were dissolved in NMP and CH_3CN, which were degassed by freeze–pump–thaw. Photocatalytically produced hydrogen was quantified using a GC-2030 (column: SH-Rt-Msieve 5A, detector: BID (Dielectric-Barrier Discharge Ionization Detector)).

General procedure for the preparation of thioketone derivatives

A magnetically stirred solution of the corresponding ketones **4–6** (1.0 mmol) in 10 mL of THF was heated to 65 °C, followed by the addition of Lawesson's reagent (0.6 mmol) in a single portion. The mixture was then heated for 4 hours under an inert nitrogen gas atmosphere. Subsequently, the solvent was removed under reduced pressure, and the residue was purified by column chromatography using an n-hexane : CH_2Cl_2 (7 : 3) eluent, yielding the desired thioketones **PS-Fc-1**, **PS-Fc-2**, and **PS-Ph** as dark violet solids.

Compound **PS-Fc-1**: 69% yield. ^{1}H-NMR (600 MHz, CD_2Cl_2): δ7.81 (d, J_{H-H} = 3.6 Hz, 1H), 7.59 (d, J_{H-H} = 8.4 Hz, 2H), 7.32–7.30 (m, 5H), 7.15–7.04 (m, 8H), 5.14 (s, 2H), 4.78 (s, 2H), 4.24 (s, 5H). $^{13}C\{^{1}H\}$-NMR (150.9 MHz, CD_2Cl_2): δ220.6, 154.3, 152.4, 148.8, 147.1, 129.8, 129.4, 126.7, 125.1, 123.8, 123.5, 122.4, 89.1, 73.5, 72.8, 72.0. DEI-MS: m/z = 556 $[M + H]^{+}$. Anal. calcd for $C_{33}H_{25}FeNS_2$: C, 71.35; H, 4.54; S, 11.54. Found C, 71.44; H, 4.68; S, 11.64.

Compound **PS-Fc-2**: 65% yield. ^{1}H-NMR (600 MHz, CD_2Cl_2): δ7.76 (d, J_{H-H} = 3.6 Hz, 1H), 7.50 (d, J_{H-H} = 8.4 Hz, 2H), 7.38 (d, J_{H-H} = 4.2 Hz, 1H), 7.31–7.28 (m, 4H), 7.25 (d, J_{H-H} = 4.2 Hz, 1H), 7.21 (d, J_{H-H} = 4.2 Hz, 1H), 7.13–7.05 (m, 9H), 5.14 (t, J_{H-H}

= 1.8 Hz), 4.79 (t, J_{H-H} = 2.1 Hz), 4.23 (s, 5H). $^{13}C\{^1H\}$-NMR (150.9 MHz, CD_2Cl_2): δ220.2, 152.5, 147.9, 147.4, 147.3, 145.4, 135.0, 129.4, 129.3, 127.2, 126.7, 126.4, 124.8, 124.5, 123.4, 123.1, 89.1, 73.7, 72.9,72.1. DEI-MS: m/z = 638 $[M + H]^+$. Anal. calcd for $C_{37}H_{27}FeNS_3$: C, 69.69; H, 4.27; S, 15.08. Found C, 69.81; H, 4.34; S, 15.22.

Compound **PS-Ph**: 79% yield. ^{1}H-NMR (600 MHz, CD_2Cl_2): δ7.67 (d, J_{H-H} = 7.2 Hz, 2H), 7.53 (t, J_{H-H} = 7.2 Hz, 1H), 7.49 (d, J_{H-H} = 8.4 Hz, 2H), 7.43–7.41 (m, 3H), 7.31–7.28 (m, 5H), 7.25 (d, J_{H-H} = 4.2 Hz, 1H), 7.22 (d, J_{H-H} = 4.2 Hz, 1H), 7.12 (d, J_{H-H} = 7.8 Hz, 4H), 7.09 (t, J_{H-H} = 7.2 Hz, 1H), 7.05 (d, J_{H-H} = 8.4 Hz, 2H). $^{13}C\{^1H\}$-NMR (150.9 MHz, CD_2Cl_2): δ220.58, 153.0, 151.4, 148.2, 147.2, 146.9, 134.6, 132.9, 130.9, 129.4, 128.5, 128.0, 127.6, 127.0, 126.5, 125.0, 124.9, 123.5, 122.9. DEI-MS: m/z = 530 $[M + H]^+$. Anal. calcd for $C_{33}H_{23}NS_3$: C, 74.82; H, 4.38; S, 18.16. Found C, 74.98; H, 4.44; S, 18.07.

General procedure for the preparation of diiron complexes

A 100 mL Schlenk flask was loaded with $Fe_3(CO)_{12}$ (0.52 mmol) along with compounds **PS-Fc-1**, **PS-Fc-2**, and **PS-Ph** (0.47 mmol), followed by the addition of 30 mL of dry THF. The resulting green solution was refluxed for 2 hours under an inert nitrogen atmosphere, during which the color gradually changed to deep red. Afterward, the solvent was evaporated under vacuum, and the crude products were purified using silica column chromatography with *n*-hexane : CH_2Cl_2 (5 : 1) as the eluent. The target products **PS-Fc-CAT-1**, **PS-Fc-CAT-2**, and **PS-Ph-CAT** were obtained from the first red-orange fractions, while **PS-Fc-CAT-3** was isolated from the second green fraction.

Complex **PS-Fc-CAT-1**: 46% yield. ^{1}H-NMR (400 MHz, CD_2Cl_2): δ7.58 (s, 1H), 7.50 (d, J_{H-H} = 8.8 Hz, 2H), 7.30 (dd, J_{H-H} = 8.4 Hz, 7.6 Hz, 4H), 7.13–7.04 (m, 8H), 5.41 (s, 1H), 4.20 (s, 5H), 4.09 (m, 2H), 3.97 (m, 1H), 3.21 (m, 1H). $^{13}C\{^1H\}$-NMR (100.6 MHz, CD_2Cl_2): δ209.7, 209.6, 165.8, 149.6, 149.0, 147.1, 135.1, 129.4, 127.5, 126.1, 125.1, 123.7, 122.5, 114.4, 91.1, 69.4, 68.5, 67.6, 67.3, 65.9, 58.2. IR (νCO): 2068, 2027, 1987 cm^{-1}. DEI-MS: m/z = 834 $[M]^+$, 778 $[M - 2CO]^+$. Anal. calcd for $C_{39}H_{25}Fe_3NO_6S_2$: C, 56.08; H, 3.02; S, 7.68. Found C, 56.19; H, 3.15; S, 7.76.

Complex **PS-Fc-CAT-2**: 41% yield. ^{1}H-NMR (600 MHz, CD_2Cl_2): δ7.52 (s, 1H), 7.49 (d, J_{H-H} = 9.0 Hz, 2H), 7.31–7.27 (m, 5H), 7.21 (d, J_{H-H} = 4.2 Hz, 1H), 7.13–7.05 (m, 8H), 5.40 (s, 1H), 4.22 (s, 5H), 4.10 (s, 2H), 3.99 (s, 1H), 3.26 (s, 1H). $^{13}C\{^1H\}$-NMR (150.9 MHz, CD_2Cl_2): δ209.6, 209.4, 165.8, 148.0, 147.3, 145.8, 142.7, 135.7, 133.6, 129.4, 127.1, 126.5, 124.8, 123.4, 123.0, 113.3, 90.9, 69.4, 68.6, 67.6, 67.4, 65.9, 58.2. IR (νCO): 2068, 2029, 1990 cm^{-1}. DEI-MS: m/z = 918 $[M + H]^+$. Anal. calcd for $C_{43}H_{27}Fe_3NO_6S_3$: C, 56.30; H, 2.97; S, 10.48. Found C, 56.44; H, 3.05; S, 10.62.

Complex **PS-Fc-CAT-3**: 27% yield. ^{1}H-NMR (600 MHz, CD_2Cl_2): δ8.55 (d, J_{H-H} = 10.2 Hz, 1H), 7.97 (d, J_{H-H} = 10.2 Hz, 1H), 7.57–7.54 (m, 3H), 7.31 (t, J_{H-H} = 7.8 Hz, 5H), 7.26 (d, J_{H-H} = 10.2 Hz, 1H), 7.14–7.09 (m, 6H), 7.04 (d, J_{H-H} = 9.0 Hz, 1H), 4.74 (s, 1H), 4.44 (d, J_{H-H} = 6.6 Hz, 2H), 4.39 (s, 1H), 4.29 (s, 5H). $^{13}C\{^1H\}$-NMR (150.9 MHz, CD_2Cl_2): δ213.6, 211.5, 209.1, 178.5, 151.9, 149.7, 148.6, 147.1, 140.0, 138.0, 129.4, 128.2, 126.8, 126.5, 125.2, 125.1, 123.8, 123.7, 122.5, 113.1, 84.5, 70.7, 69.9, 69.4, 68.8, 68.6, 66.0. IR (νCO): 2043, 2035, 2000, 1946 cm^{-1}. DEI-MS: m/z = 918 $[M]^+$, 890 $[M - CO]^+$, 862 $[M - 2CO]^+$, 834 $[M - 3CO]^+$, 806 $[M - 4CO]^+$, 778 $[M - 5CO]^+$. Anal. calcd for $C_{43}H_{28}Fe_3NO_6S_3$: C, 56.23; H, 3.07; S, 10.47. Found C, 56.35; H, 3.18; S, 10.53.

Complex **PS-Ph-CAT**: 38% yield. ^{1}H-NMR (400 MHz, CD_2Cl_2): δ7.64 (s, 1H), 7.48 (d, J_{H-H} = 8.8 Hz, 2H), 7.29 (t, J_{H-H} = 7.8 Hz, 4H), 7.22–7.17 (m, 5H), 7.12–7.03 (m, 8H), 6.60 (dd, J_{H-H} = 2.8, 6.4 Hz, 2H), 5.57 (s, 1H). $^{13}C\{^1H\}$-NMR (100.6 MHz, CD_2Cl_2): δ209.4, 209.2, 168.8, 148.0, 147.3, 146.1, 141.9, 135.6, 129.4, 128.3, 128.1, 127.7, 127.0, 126.5, 126.2, 124.8, 123.5, 123.0,110.8, 60.06. APCI-MS (negative mode): m/z = 724 $[M - 3CO]^-$, 640 $[M - 6CO]^-$. Anal. calcd for $C_{39}H_{23}Fe_2NO_6S_3$: C, 57.87; H, 2.86; S, 11.88. Found C, 57.95; H, 2.92; S, 11.82.

Conflicts of interest

There are no conflicts of interest to declare.

Data availability

The data supporting this article have been included as part of the SI. Supplementary information is available. See DOI: https://doi.org/10.1039/d5qi01191d.

CCDC 2445996 and 2445997 contain the supplementary crystallographic data for this paper.[73a,b]

Acknowledgements

I. B. is thankful to the Deutsche Akademischer Austauschdienst (DAAD) for a scholarship. M. W. acknowledges the Deutsche Forschungsgemeinschaft (German Research Foundation) *via* TRR234 CATALIGHT, Projektnummer 364549901 (TP: Z2). K. R. greatfully acknowledges the financial support by the Fonds der Chemischen Industrie (FCI) in the form of a Kekulé Scholarship (115571). We thank Dr. Stephan Kupfer (Uni Jena) for the fruitful discussions on the theoretical approaches and Prof. Christoph van Wüllen (RPTU) for the support in using the computation resources at RPTU. H. A.-F. acknowledges the financial support provided by the Deanship of Scientific Research at the Hashemite University (38/2024).

References

1 D. G. Nocera, Solar Fuels and Solar Chemicals Industry, *Acc. Chem. Res.*, 2017, **50**, 616–619.
2 N. S. Lewis, Aspects of Science and Technology in Support of Legal and Policy Frameworks Associated with a Global Carbon Emissions-Control Regime, *Energy Environ. Sci.*, 2016, **6**, 2172–2176.

3 H. B. Gray, Powering the Planet with Solar Fuel, *Nat. Chem.*, 2009, **1**, 7.
4 H. Ishaq, I. Dincer and C. Crawford, A Review on Hydrogen Production and Utilization: Challenges and Opportunities, *Int. J. Hydrogen Energy*, 2022, **47**, 26238–26264.
5 L.-Z. Wu, B. Chen, Z.-J. Li and C.-H. Tung, Enhancement of the Efficiency of Photocatalytic Reduction of Protons to Hydrogen via Molecular Assembly, *Acc. Chem. Res.*, 2014, **47**, 2177–2185.
6 Z. Han, L. Shen, W. W. Brennessel, P. L. Holland and R. Eisenberg, Nickel Pyridinethiolate Complexes as Catalysts for the Light-Driven Production of Hydrogen from Aqueous Solutions in Noble-Metal-Free Systems, *J. Am. Chem. Soc.*, 2013, **135**, 14659–14669.
7 L. Duan, F. Bozoglian, S. Mandal, B. Stewart, T. Privalov, A. Llobet and L. Sun, A Molecular Ruthenium Catalyst with Water-Oxidation Activity Comparable to that of Photosystem II, *Nat. Chem.*, 2012, **4**, 418–423.
8 Y. Halpin, M. T. Pryce, S. Rau, D. Dini and J. G. Vos, Recent Progress in the Development of Bimetallic Photocatalysts for Hydrogen Generation, *Dalton Trans.*, 2013, **42**, 16243–16254.
9 P. D. Frischmann, K. Mahata and F. Wurther, Powering the Future of Molecular Artificial Photosynthesis with Lght-Harvesting Metallosupramolecular Dye Assemblies, *Chem. Soc. Rev.*, 2013, **42**, 1847–1870.
10 W. T. Eckenhoff and R. Eisenberg, Molecular Systems for Light Driven Hydrogen Production, *Dalton Trans.*, 2012, **41**, 13004–13021.
11 M. Schulz, M. Karnahl, M. Schwalbe and J. G. Vos, The Role of the Bridging Ligand in Photocatalytic Supramolecular Assemblies for the Reduction of Protons and Carbon Dioxide, *Coord. Chem. Rev.*, 2012, **256**, 1682–1705.
12 W. Lubitz, H. Ogata, O. Rüdiger and E. Reijerse, Hydrogenases, *Chem. Rev.*, 2014, **114**, 4081–4148.
13 M. W. Adams, The Structure and Mechanism of Iron-hydrogenases, *Biochim. Biophys. Acta*, 1990, **1020**, 115–145.
14 M. Frey, Hydrogenases: Hydrogen-Activating Enzymes, *ChemBioChem*, 2002, **3**, 153–160.
15 J. W. Peters, W. N. Lanzilotta, B. J. Lemon and L. C. Seefeldt, X-ray Crystal Structure of the Fe-Only Hydrogenase (CpI) from Clostridium pasteurianum to 1.8 Angstrom Resolution, *Science*, 1998, **282**, 1853–1858.
16 A. Adamska-Venkatesh, S. Roy, J. F. Siebel, T. R. Simmons, M. Fontecave, V. Artero, E. Reijerse and W. Lubitz, Spectroscopic Characterization of the Bridging Amine in the Active Site of [FeFe] Hydrogenase Using Isotopologues of the H-cluster, *J. Am. Chem. Soc.*, 2015, **137**, 12744–12747.
17 H.-J. Fan and M. B. Hall, A Capable Bridging Ligand for Fe-only Hydrogenase: Density Functional Calculations of a Low-Energy Route for Heterolytic Cleavage and Formation of Dihydrogen, *J. Am. Chem. Soc.*, 2001, **123**, 3828–3829.
18 L. R. Almazahreh, F. Arrigoni, H. Abul-Futouh, M. Elkhateeb, H. Görls, C. Elleouet, P. Schollhammer, L. Bertini, L. De Gioia, M. Rudolph, G. Zampella and W. Weigand, Proton Shuttle Mediated by $(SCH_2)_2P{=}O$ Moiety in [FeFe]-Hydrogenase Mimics: Electrochemical and DFT Studies, *ACS Catal.*, 2021, **11**, 7080–7098.
19 H. Abul-Futouh, D. Costabel, K. Hotzel, P. Liebing, H. Görls, W. Weigand and K. Peneva, Mono- and Di-Substituted [FeFe]-Hydrogenase H-cluster Mimics Bearing the 3,4-dimercaptobenzaldehyde Bridge Moiety: Insight into Synthesis, Characterization and Electrochemical Investigations, *Inorg. Chim. Acta*, 2023, **551**, 121469.
20 S. Gao, W. Fan, Y. Liu, D. Jiang and Q. Duan, Artificial Water-Soluble Systems Inspired by [FeFe]-Hydrogenases for Electro- and Photocatalytic Hydrogen Production, *Int. J. Hydrogen Energy*, 2020, **45**, 4305–4327.
21 S. Gao, Y. Liu, Y. Shao, D. Jiang and Q. Duan, Iron Carbonyl Compounds with Aromatic Dithiolate Bridges as Organometallic Mimics of [FeFe] Hydrogenases, *Coord. Chem. Rev.*, 2020, **402**, 213081, and references cited therein.
22 Y. Li and T. B. Rauchfuss, Synthesis of Diiron(I) Dithiolato Carbonyl Complexes, *Chem. Rev.*, 2016, **116**, 7043–7077, and references cited therein.
23 H. Abul-Futouh, L. R. Almazahreh, S. J. Abaalkhail, H. Görls, S. T. Stripp and W. Weigand, Ligand Effects on Structural, Protophilic and Reductive Features of Stannylated Dinuclear Iron Dithiolato Complexes, *New J. Chem.*, 2021, **45**, 36–44.
24 I. Basma, H. Abul-Futouh, S. J. Abaalkhail, P. Liebing and W. Weigand, [FeFe]-Hydrogenase H-Cluster Mimics Mediated by Ferrocenyl Hetaryl Thioketone Derivatives, *J. Mol. Struct.*, 2024, **1295**, 136630.
25 Z.-Y. Ma, X.-F. Liu, B. Jin, D. Wang and P.-H. Zhao, Substituent Effects of Tertiary Phosphines on the Structures and Electrochemical Performances of Azadithiolato-Bridged Diiron Model Complexes of [FeFe]-Hydrogenases, *Appl. Organomet. Chem.*, 2022, **36**, e6751.
26 T. Yu, Y. Zeng, J. Chen, Y.-Y. Li, G. Yang and Y. Li, Exceptional Dendrimer-Based Mimics of Diiron Hydrogenase for the Photo-chemical Production of Hydrogen, *Angew. Chem., Int. Ed.*, 2013, **52**, 5631–5635.
27 K. A. Brown, M. B. Wilker, M. Boehm, G. Dukovic and P. W. King, Characterization of Photochemical Processes for H_2 Production by CdS Nanorod–[FeFe] Hydrogenase Complexes, *J. Am. Chem. Soc.*, 2012, **134**, 5627–5636.
28 W.-G. Wang, F. Wang, H.-Y. Wang, G. Si, C.-H. Tung and L.-Z. Wu, Photocatalytic Hydrogen Evolution by [FeFe] Hydrogenase Mimics in Homogeneous Solution, *Chem. - Asian J.*, 2010, **5**, 1796–1803.
29 F. Wang, W.-G. Wang, H.-Y. Wang, G. Si, C.-H. Tung and L.-Z. Wu, Artificial Photosynthetic Systems Based on [FeFe]-Hydrogenase Mimics: The Road to High Efficiency for Light-Driven Hydrogen Evolution, *ACS Catal.*, 2012, **2**, 407–416.
30 S. Fukuzumi, Y. Lee and W. Nam, Thermal and Photocatalytic Production of Hydrogen with Earth-Abundant Metal Complexes, *Coord. Chem. Rev.*, 2018, **355**, 54–73.
31 J. Amaro-Gahete, M. V. Pavliuk, H. Tian, D. Esquivel, F. J. Romero-Salguero and S. Ott, Catalytic Systems Mimicking the [FeFe]-Hydrogenase Active Site for Visible-

Light-Driven Hydrogen Production, *Coord. Chem. Rev.*, 2021, **448**, 214172.

32 S. Ott, M. Kritikos, B. Åkermark and L. Sun, Synthesis and structure of a biomimetic model of the iron hydrogenase active site covalently linked to a ruthenium photosensitizer, *Angew. Chem., Int. Ed.*, 2003, **42**, 3285–3288.

33 X. Li, M. Wang, S. Zhang, J. Pan, Y. Na, J. Liu, B. Åkermark and L. Sun, Noncovalent assembly of a metalloporphyrin and an iron hydrogenase active-site model: photo-induced electron transfer and hydrogen generation, *J. Phys. Chem. B*, 2008, **112**, 8198–8202.

34 L.-C. Song, M.-Y. Tang, F.-H. Su and Q.-M. Hu, A Biomimetic model for the active site of iron-only hydrogenases covalently bonded to a porphyrin photosensitizer, *Angew. Chem., Int. Ed.*, 2006, **45**, 1130–1133.

35 L.-C. Song, L.-X. Wang, M.-Y. Tang, C.-G. Li, H.-B. Song and Q.-M. Hu, Synthesis, structure, and photoinduced catalysis of [FeFe]-hydrogenase active site models covalently linked to a porphyrin or metalloporphyrin moiety, *Organometallics*, 2009, **28**, 3834–3841.

36 A. P. S. Samuel, D. T. Co, C. L. Stern and M. R. Wasielewski, Ultrafast photodriven intramolecular electron transfer from a zinc porphyrin to a readily reduced diiron hydrogenase model complex, *J. Am. Chem. Soc.*, 2010, **132**, 8813–8815.

37 L. Sun, B. Akermark and S. Ott, Iron hydrogenase active site mimics in supramolecular systems aiming for light-driven hydrogen production, *Coord. Chem. Rev.*, 2005, **249**, 1653–1663.

38 J. Ekström, M. Abrahamsson, C. Olson, J. Bergquist, F. B. Kaynak, L. Eriksson, L. Sun, H.-C. Becker, B. Åkermark, L. Hammarström and S. Ott, Bio-inspired, side-on attachment of a ruthenium photosensitizer to an iron hydrogenase active site model, *Dalton Trans.*, 2006, 4599–4606.

39 W. Gao, J. Liu, W. Jiang, M. Wang, L. Weng, B. Åkermark and L. Sun, An azadithiolate bridged Fe_2S_2 complex as active site model of FeFehydrogenase covalently linked to a Re(CO)3(bpy)(py) photosensitizer aiming for light-driven hydrogen production, *C. R. Chim.*, 2008, **11**, 915–921.

40 A. M. Kluwer, R. Kapre, F. Hartl, M. Lutz, A. L. Spek, A. M. Brouwer, P. W. N. M. van Leeuwen and J. N. H. Reek, Self-assembled biomimetic [2Fe2S]-hydrogenase based photocatalyst for molecular hydrogen evolution, *Proc. Natl. Acad. Sci. U. S. A.*, 2009, **106**, 10460–10465.

41 H.-H. Cui, M.-Q. Hu, H.-M. Wen, G.-L. Chai, C.-B. Ma, H. Chen and C.-N. Chen, Efficient [FeFe] hydrogenase mimic dyads covalently linking to iridium photosensitizer for photocatalytic hydrogen evolution, *Dalton Trans.*, 2012, **41**, 13899–13907.

42 S. Ott, M. Borgström, M. Kritikos, R. Lomoth, J. Bergquist, B. Åkermark, L. Hammarström and L. Sun, Model of the iron hydrogenase active site covalently linked to a ruthenium photosensitizer: synthesis and photophysical properties, *Inorg. Chem.*, 2004, **43**, 4683–4692.

43 S. Gao, W.-Y. Zhang, Q. Duan, Q.-C. Liang, D.-Y. Jiang, J.-X. Zhao and J.-H. Hou, An artificial [FeFe]-hydrogenase mimic with organic chromophore-linked thiolate bridges for the photochemical production of hydrogen, *Chem. Pap.*, 2017, **71**, 617–625.

44 R. Goy, U.-P. Apfel, C. Elleouet, D. Escudero, M. Elstner, H. Görls, J. Talarmin, P. Schollhammer, L. González and W. Weigand, A Silicon-heteroaromatic system as photosensitizer for light-driven hydrogen production by hydrogenase mimics, *Eur. J. Inorg. Chem.*, 2013, 4466–4472.

45 R. Goy, L. Bertini, T. Rudolph, S. Lin, M. Schulz, G. Zampella, B. Dietzek, F. H. Schacher, L. De Gioia, K. Sakai and W. Weigand, Photocatalytic hydrogen evolution driven by [FeFe] hydrogenase models tethered to fluorene and silafluorene sensitizers, *Chem. – Eur. J.*, 2017, **23**, 334–345.

46 P. Buday, C. Kasahara, E. Hofmeister, D. Kowalczyk, M. K. Farh, S. Riediger, M. Schulz, M. Wächtler, S. Furukawa, M. Saito, D. Ziegenbalg, S. Gräfe, P. Bäuerle, S. Kupfer, B. Dietzek-Ivanšić and W. Weigand, Activating a [FeFe] Hydrogenase Mimic for Hydrogen Evolution under Visible Light, *Angew. Chem., Int. Ed.*, 2022, **61**, e202202079.

47 A. Q. Daraosheh, H. Abul-Futouh, N. Murakami, K. M. Ziems, H. Görls, S. Kupfer, S. Gräfe, A. Ishii, M. Celeda, G. Mloston and W. Weigand, Novel [FeFe]-Hydrogenase Mimics: Unexpected Course of the Reaction of Ferrocenyl α-Thienyl Thioketone with $Fe_3(CO)_{12}$, *Materials*, 2022, **15**, 2867.

48 I. Basma, S. J. Abaalkhail, H. Abul-Futouh, P. Liebing, P. Matczak, G. Mloston and W. Weigand, Tropothione as a remarkable 8π electron substrate in complexation reaction with $Fe_3(CO)_{12}$: Experimental and computational studies, *Inorg. Chem. Commun.*, 2025, **174**, 114025.

49 X. Wu, W. Wu, C. Cui, J. Zhao and M. Wu, Preparation of Bodipy–ferrocene dyads and modulation of the singlet/triplet excited state of bodipy *via* electron transfer and triplet energy transfer, *J. Mater. Chem. C*, 2016, **4**, 2843–2853.

50 M. Supur, M. E. El-khouly, J. H. Seok, J. H. Kim, K.-Y. Kay and S. Fukuzumi, Efficient Electron Transfer Processes of the Covalently Linked Perylenediimide–Ferrocene Systems: Femtosecond and Nanosecond Transient Absorption Studies, *J. Phys. Chem. C*, 2010, **114**, 10969–10977.

51 D. M. S. C. Dissanayake, M. H. Dinh, J. J. Kuchta and A. K. Vannucci, Ferrocene-Mediated Photochemical Reduction of Naphthol to Generate Hydrogen, *Chem. – Eur. J.*, 2025, e01540.

52 R. Itagki, S.-Y. Takizawa, H.-C. Chang and A. Nakada, Light-induced electron transfer/phase migration of a redox mediator for photocatalytic C–C coupling in a biphasic solution, *Dalton Trans.*, 2022, **51**, 9467–9476.

53 E. Maligaspe, M. R. Hauwiller, Y. V. Zatsikha, J. A. Hinke, P. V. Solntsev, D. A. Blank and V. N. Nemykin, Redox and Photoinduced Electron-Transfer Properties in Short Distance Organoboryl Ferrocene-Subphthalocyanine Dyads, *Inorg. Chem.*, 2014, **53**, 9336–9347.

54 H. Miyake, T. Tajima and Y. Takaguchi, Synthesis and Light-absorption Characteristics of Thiophene Derivatives

Bearing Ferrocenylthiocarbonyl Groups, *Chem. Lett.*, 2017, **46**, 48–50.

55 P. Kumaresan, Y.-Y. Liu, S. Vegiraju, Y. Ezhumalai, H.-C. Yu, S. L. Yau, M.-C. Chen and T.-C. Lin, Synthesis and Characterization of Two-Photon ActiveChromophores Based on Tetrathienoacene (TTA) and Dithienothiophene (DTT), *Chem. - Asian J.*, 2015, **10**, 1640–1646.

56 Y. Li, J. Hu, G. He, H. Zhu, X. Wang, Q. Guo, A. Xia, Y. Lin, J. Wang and X. Zhan, Influence of Thiophene Moiety on the Excited State Properties of Push–Pull Chromophores, *J. Phys. Chem. C*, 2016, **120**(26), 13922–13930.

57 S. Roquet, A. Cravino, P. Leriche, O. Alévêque, P. Frère and J. Roncali, Triphenylamine–thienylenevinylene hybrid systems with internal charge transfer as donor materials for heterojunction solar cells, *J. Am. Chem. Soc.*, 2006, **128**, 3459–3466.

58 H. Kanato, K. Takimiya, T. Otsubo, Y. Aso, T. Nakamura, Y. Araki and O. Ito, Synthesis and photophysical properties of ferrocene–oligothiophene–fullerene triads, *J. Org. Chem.*, 2004, **69**, 7183–7189.

59 X. Wu, W. Wu, X. Cui, J. Zhao and M. Wu, Preparation of Bodipy–ferrocene dyads and modulation of the singlet/triplet excited state of bodipy via electron transfer and triplet energy transfer, *J. Mater. Chem. C*, 2016, **4**, 2843–2853.

60 H. Wang, G. Si, W. Cao, W. Wang, Z. Li, F. Wang, C. Tung and L. Wu, A triad [FeFe] hydrogenase system for light-driven hydrogen evolution, *Chem. Commun.*, 2011, **47**, 8406–8408.

61 R. Giasson, E. J. Lee, X. Zhao and M. S. Wrighton, Inter-and intramolecular quenching of the singlet excited state of porphyrins by ferrocene, *J. Phys. Chem.*, 1993, **97**, 2596–2601.

62 C. Kasahara, K. Rediger, M. Micheel, P. Liebing, S. Gräfe, S. Kupfer, M. Wächtler and W. Weigand, Molecular Dyad vs Multi–Component Approach–Photocatalytic Hydrogen Evolution by Combining Oligothiophene Photosensitizers with [FeFe]–Hydrogenase Mimics, *ChemCatChem*, 2024, **16**, e202400247.

63 A. Farmilo and F. Wilkinson, Triplet state quenching by ferrocene, *Chem. Phys. Lett.*, 1975, **34**, 575–580.

64 G. Mlostoń, R. Hamera and H. Heimgartner, Synthesis of Ferrocenyl Thioketones and their Reactions with Diphenyldiazomethane, *Phosphorus, Sulfur Silicon Relat. Elem.*, 2015, **190**, 2125–2133.

65 J. Skiba, R. Karpowicz, I. Szabó, B. Therrien and K. Kowalski, Synthesis and anticancer activity studies of ferrocenyl-thymine-3,6-dihydro-2*H*-thiopyranes - A new class of metallocene-nucleobase derivatives, *J. Organomet. Chem.*, 2015, **794**, 216–222.

66 G. Mlostoń, R. Hamera-Fałdyga, M. Celeda and H. Heimgartner, Efficient synthesis of ferrocifens and other ferrocenyl-substituted ethylenes *via* a 'sulfur approach', *Org. Biomol. Chem.*, 2018, **16**, 4350–4356.

67 G. Mlostoń, R. Hamera-Fałdyga, K. Urbaniak, W. Weigand and H. Heimgartner, A convenient access to 1,2-diferrocenyl-substituted ethylenes via [3 + 2]-cycloelimination of 2-silylated 4,4,5,5-tetrasubstituted 1,3-dithiolanes, *J. Sulfur Chem.*, 2018, **39**, 516–524.

68 N. Murakami, H. Miyake, T. Tajima, K. Nishikawa, R. Hirayama and Y. Takaguchi, Enhanced Photosensitized Hydrogen Production by Encapsulation of Ferrocenyl Dyes into Single-Walled Carbon Nanotubes, *J. Am. Chem. Soc.*, 2018, **140**, 3821–3824.

69 G. M. Sheldrick, SHELXT-Integrated Space-Group and Crystal-Structure Determination, *Acta Crystallogr.*, 2015, **A71**, 3–8.

70 G. M. Sheldrick, Crystal Structure Refinement with SHELXL, *Acta Crystallogr.*, 2015, **C71**, 3–8.

71 O. V. Dolomanov, L. J. Bourhis, R. J. Gildea, J. A. K. Howard and H. Puschmann, OLEX2: A Complete Structure Solution, Refinement and Analysis Program, *J. Appl. Crystallogr.*, 2009, **42**, 339–341.

72 *Bruker AXS 2001, Apex4 and SADABS*, Bruker AXS Inc., Madison, Wisconsin, USA.

73 (*a*) I. Basma, K. Rediger, C. Kasahara, H. Abul-Futouh, M. Micheel, M. K. Farh, P. Köhler, G. Mlostoń, M. Wächtler and W. Weigand, CCDC 2445996: Experimental Crystal Structure Determination, 2025, DOI: **10.5517/ccdc.csd.cc2n3835**; (*b*) I. Basma, K. Rediger, C. Kasahara, H. Abul-Futouh, M. Micheel, M. K. Farh, P. Köhler, G. Mlostoń, M. Wächtler and W. Weigand, CCDC 2445997: Experimental Crystal Structure Determination, 2025, DOI: **10.5517/ccdc.csd.cc2n3846**.